4-10-2014

A Chandra Grating Observation of the Dusty Wolf-Rayet Star WR 48a

Svetozar A. Zhekov
Space Research and Technology Institute, Sofia, Bulgaria

Marc Gagne
West Chester University of Pennsylvania, mgagne@wcupa.edu

Stephen L. Skinner
University of Colorado Boulder

Recommended Citation

Zhekov, S. A., Gagne, M., & Skinner, S. L. (2014). A Chandra Grating Observation of the Dusty Wolf-Rayet Star WR 48a. *The Astrophysical Journal, 785*(1), 1-8. http://dx.doi.org/10.1088/0004-637X/785/1/8

A *CHANDRA* GRATING OBSERVATION OF THE DUSTY WOLF–RAYET STAR WR 48a

Svetozar A. Zhekov[1], Marc Gagné[2], and Stephen L. Skinner[3]

[1] Space Research and Technology Institute, Akad. G. Bonchev Str., bl.1, Sofia 1113, Bulgaria; szhekov@space.bas.bg
[2] Department of Geology and Astronomy, West Chester University, West Chester, PA 19383, USA; mgagne@wcupa.edu
[3] CASA, University of Colorado, Boulder, CO 80309, USA; stephen.skinner@colorado.edu

ABSTRACT

We present results of a *Chandra* High-Energy Transmission Grating (HETG) observation of the carbon-rich Wolf–Rayet (WR) star WR 48a. These are the first high-resolution spectra of this object in X-ray. Blueshifted centroids of the spectral lines of ~-360 km s^{-1} and line widths of 1000–1500 km s^{-1} (FWHM) were deduced from the analysis of the line profiles of strong emission lines. The forbidden line of Si XIII is strong and not suppressed, indicating that the rarified 10–30 MK plasma forms far from strong sources of far-ultraviolet emission, most likely in a wind collision zone. Global spectral modeling showed that the X-ray spectrum of WR 48a suffered higher absorption in the 2012 October *Chandra* observation compared with a previous 2008 January *XMM-Newton* observation. The emission measure of the hot plasma in WR 48a decreased by a factor $\sim$3 over the same period of time. The most likely physical picture that emerges from the analysis of the available X-ray data is that of colliding stellar winds in a wide binary system with an elliptical orbit. We propose that the unseen secondary star in the system is another WR star or perhaps a luminous blue variable.

Key words: shock waves – stars: individual (WR48a) – stars: Wolf–Rayet – X-rays: stars

Online-only material: color figures

1. INTRODUCTION

WR 48a is a carbon-rich (WC) Wolf–Rayet (WR) star with a WC8 spectral classification (van der Hucht 2001) that was discovered in a near-infrared survey by Danks et al. (1983). This WC star is located inside the G305 star-forming region in the Scutum Crux arm of the Galaxy. Its proximity (within 2′) to the two compact infrared clusters Danks 1 and 2 suggests that WR 48a likely originates from one or the other (Danks et al. 1984). The optical extinction toward WR 48a is very high, $A_V = 9.2$ mag (Danks et al. 1983), and only a small part of it is due to circumstellar material (Baume et al. 2009). The distance to WR 48a is not yet well constrained, and various studies provide a range of 1.21–4 kpc (e.g., van der Hucht 2001; Baume et al. 2009; Danks et al. 1983).

The evolution of its infrared emission suggests that WR 48a is a long-period episodic dust maker (Williams 1995). This was confirmed by a recent study that revealed recurrent dust formation on a timescale of more than 32 yr, which also indicates that WR 48a is very likely a wide colliding-wind binary (Williams et al. 2012). However, the interpretation of the nature of WR 48a may not be straightforward. Recently, Hindson et al. (2012) reported the detection of a thermal radio source (spectral index $\alpha = 0.6$, $F_\nu \propto \nu^\alpha$) associated with WR 48a. As a rule, wide colliding-wind binaries are nonthermal radio sources (Dougherty & Williams 2000).

Nevertheless, the binary nature of WR 48a is further supported by its X-ray characteristics. Analysis of the *XMM-Newton* spectra of WR 48a showed that its X-ray emission is of thermal origin, and this is the most X-ray luminous WR star in the Galaxy detected so far, after the black hole candidate Cyg X-3 (Zhekov et al. 2011). The latter is valid, provided that WR 48a is associated with the open clusters Danks 1 and 2, and it is thus located at the distance of $\sim$4 kpc (Danks et al. 1983).

It is important to recall that all of the aforementioned X-ray observations of a small sample of presumed single WC stars have yielded only nondetections, demonstrating that they are X-ray faint or X-ray quiet (Oskinova et al. 2003; Skinner et al. 2006). Therefore, the high X-ray luminosity of the WC star WR 48a is a clear sign that it is not a single star, and it is very likely that its enhanced X-ray emission originates from the interaction region of the winds of two massive binary components (Prilutskii & Usov 1976; Cherepashchuk 1976).
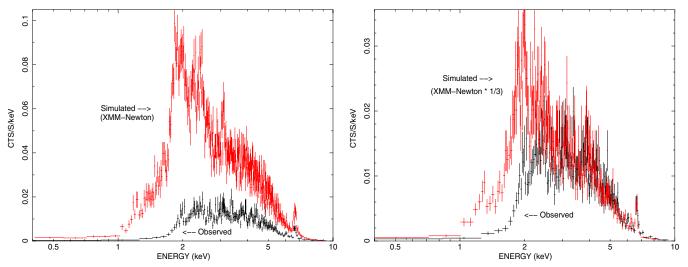
In this paper, we report results from the first grating observation of the dusty WR star WR 48a. In Section 2, we briefly review the *Chandra* High-Energy Transmission Grating (HETG) observation. In Section 3, we present an overview of the X-ray spectra. In Section 4, we analyze the profiles and ratios of strong X-ray emission lines. In Section 5, we present the results from the global spectral fits. We discuss the results from our analysis in Section 6 and list our conclusions in Section 7.

2. OBSERVATIONS AND DATA REDUCTION

WR 48a was observed with the *Chandra* HETG and ACIS-S detector on 2012 October 12 (*Chandra* ObsId: 13636) with a total effective exposure of 98.6 ks. Following the Science Threads for Grating Spectroscopy in the Chandra Interactive Analysis of Observations[4] 4.4.1 data analysis software, the first-order Medium Energy Grating/High Energy Grating (MEG/HEG) and the zeroth-order HETG spectra were extracted.[5] The total source counts were 2083 (MEG), 1456 (HEG) and 4478 (HETG-0), where the MEG and HEG counts are for the +1 and −1 orders combined. The *Chandra* calibration database CALDB v.4.5.0 was used to construct the response matrices and the ancillary response files. For the spectral analysis in this study, we made use of version 11.3.2 of XSPEC (Arnaud 1996).

---

[4] For details, see http://cxc.harvard.edu/ciao.
[5] We note that the associated errors for the grating spectra are based on Gehrels (1986). This is the default statistical error for extracting such spectra with the Chandra Interactive Analysis of Observations because, as a rule, the grating spectra have a small number of counts in the individual spectral bins.

Figure 1. *Chandra* HETG-0 spectrum of WR 48a (black) and the simulated spectrum in XSPEC using the optically thin plasma model that perfectly fits the *XMM-Newton* EPIC spectra (red). The original spectra are shown in the left panel while in the right panel the simulated spectrum has a reduced flux (emission measure) by a factor of three.

(A color version of this figure is available in the online journal.)

3. AN OVERVIEW OF THE X-RAY SPECTRA

As shown in the analysis of the *XMM-Newton* data (Zhekov et al. 2011), WR 48a is the most X-ray luminous WR star in the Galaxy, after the black hole candidate Cyg X-3, and its spectrum is subject to considerable X-ray absorption. The 5 yr time interval between the *XMM-Newton* and *Chandra* observations provides an opportunity to search for any changes of the X-ray emission that may have occurred. From such a comparison, we can immediately conclude that the source has become weaker and its X-ray absorption has increased, as illustrated by the following.

Given that the previous *XMM-Newton* observation provided undispersed spectra of WR 48a, it is natural to compare them with the undispersed HETG-0 spectrum from the new *Chandra* observation. We used the two-shock model that perfectly fits the *XMM-Newton* spectra (see Table 1 in Zhekov et al. 2011) to simulate in XSPEC the expected HETG-0 spectrum by adopting the response matrix and the ancillary file as derived for the *Chandra* observation (see Section 2). This procedure yields a predicted HETG-0 spectrum that assumes there were no changes in the X-ray emission of WR 48a between the two observations. Figure 1 shows two versions of the simulated HETG-0 spectrum: one with the nominal values of the two-shock model (absorption, temperature, emission measure) based on the *XMM-Newton* results and one with the emission measure (intrinsic flux) decreased by a factor of three (absorption and temperature are kept the same). By comparing the left and right panels in Figure 1, we conclude that the absorption was higher during the 2012 *Chandra* observation than during the 2008 *XMM-Newton* observation. In addition, the rescaled *Chandra* spectrum in the right panel of Figure 1 shows that the emission measure during the *Chandra* observation was about a factor of ~3 lower than during the *XMM-Newton* observation. In Section 5, we further analyze and discuss this overall change in the X-ray spectrum of WR 48a.

4. SPECTRAL LINES

Because of the decrease in X-ray brightness of WR 48a between the two observations, we obtained fewer counts in

the *Chandra* spectra than were anticipated. As a result, we were able to derive reliable information for only a few of the brightest lines in the grating spectra. We re-binned the first-order MEG and HEG spectra every two bins to improve the photon statistics in the individual spectral bins.[6] For the Si XIII, S XV, and Fe XXV He-like triplets, we fitted a sum of three Gaussians and a constant continuum. The centers of the triplet components were held fixed according to the AtomDB database (Atomic Data for Astrophysicists)[7] and all components shared the same line width and line shift. Similarly (with a sum of two Gaussians), we fitted the Si XIV and S XVI H-like doublets, but the component intensity ratios were fixed at their atomic data values.
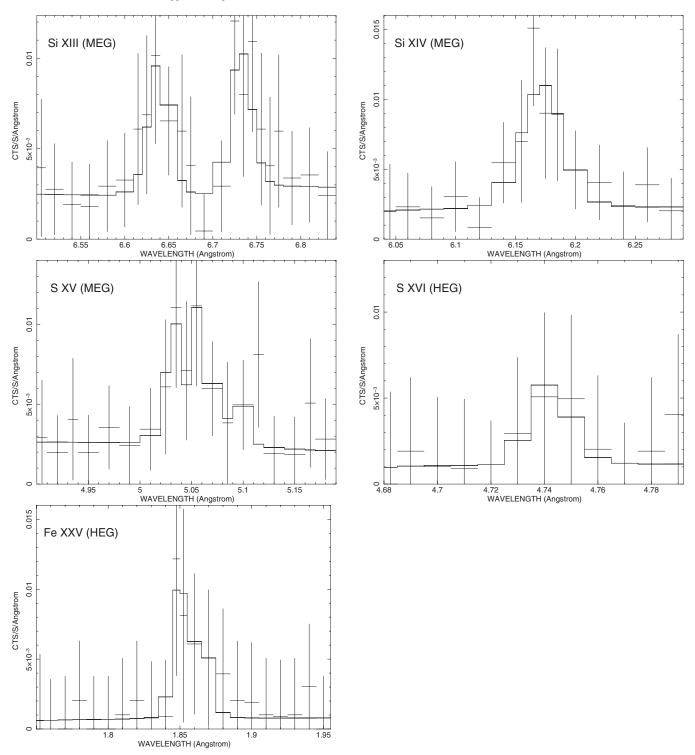
Figures 2 and 3 and Table 1 show the results from the fits to the line profiles in the X-ray grating spectra of WR 48a. Only the Si XIII and Si XIV lines are of acceptable quality for determining whether significant line centroid shifts are present (see Figure 2). These two lines are blueshifted in the 2012 October *Chandra* observation. This is further supported by results for the S XV line, but the data quality in that part of the spectrum is not as good (e.g., near the forbidden line at ~5.1 Å). The other two lines that were analyzed show a redshift (S XVI) or a zero-shift (Fe XXV), but this may well be a result of their poorer photon statistics. Similarly, the Si XIII and Si XIV line results show line broadening of about 1000–1500 km s^{-1}, whereas the lines at shorter wavelengths seem to be unresolved in the MEG and HEG spectra (e.g., their line widths are consistent with a zero width, namely, the lower limit of the 1σ confidence interval is zero; see Table 1), which is again likely a result of the lower data quality (fewer counts) in these lines.

We checked all of the fit results by further improving the photon statistics in individual spectral bins. In particular, we re-binned the spectra every four bins at the expense of some loss of spectral resolution: the bin size after re-binning was 0.02 Å (MEG) and 0.01 Å (HEG). The fits to these heavily

---

[6] The bin sizes of the re-binned spectra are 0.01 Å and 0.005 Å for the MEG and HEG spectra, respectively. The resolution element (FWHM) is 0.023 Å (MEG) and 0.012 Å (HEG): see Table 8.1 in the *Chandra* Proposer's Observatory Guide (POG);
http://asc.harvard.edu/proposer/POG/html/index.html
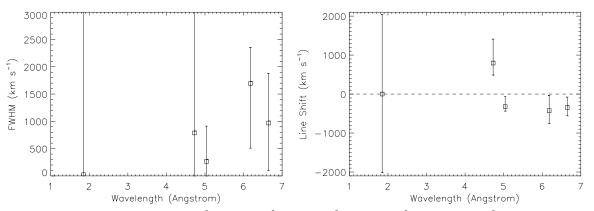[7] For AtomDB, see http://www.atomdb.org/

Figure 2. Line profile fits to some H-like doublets (Si XIV, S XVI) and He-like triplets (Si XIII, S XV, Fe XXV) in the HEG/MEG first-order spectra of WR 48a. The total number of counts (line + continuum) in all components of a line complex (doublet or triplet) are 118 ± 19 (Si XIII), 81 ± 15 (Si XIV), 89 ± 16 (S XV), 16 ± 11 (S XVI), 28 ± 12 (Fe XXV). For presentation purposes, the spectra were slightly re-binned with respect to the original binning used in the fits (see Section 4).

re-binned spectra confirmed our basic findings, that is, blueshifted Si XIII, Si XIV and S XV lines. As expected from the coarser binning, the widths of all of the lines were consistent with a zero width, namely, the lower limit of the 1σ confidence interval was zero.

We also adopted a different approach to the line profile fitting by making use of a statistic different from the standard χ^2-statistic. We made use of the implementation of the Cash

statistic (Cash 1979) in XSPEC. The fit results were very similar to those discussed earlier: the fit parameters were within 5%–15% of the values with χ^2 statistic, and they were more tightly constrained (the errors were 45%–60% of the values derived if using the standard χ^2-statistic; see Table 1).

To check whether the derived results from the line profile fits are sensitive to the local level of continuum, we performed a global-continuum fit. We *simultaneously* fitted all of the

Figure 3. Spectral line parameters of WR 48a: Fe xxv (1.85 Å), S xvi (4.73 Å), S xv (5.04 Å), Si xiv (6.18 Å), and Si xiii (6.65 Å). Left panel: FWHM. Right panel: the shift of the centroid of the spectral lines. The error bars correspond to the 1σ errors from the line profile fits (see Table 1).

Table 1
Line Parameters

Line	$\lambda_{\rm lab}$[a] (Å)	FWHM[b] (km s^{-1})	Line Shift[c] (km s^{-1})	Flux[d]	Ratio (AtomDB)
Fe xxv K$_\alpha$	1.850	23^{+6001}_{-23}	0^{+2040}_{-2013}	$12.26^{+5.59}_{-6.40}$	
(i/r)[e]				$0.43^{+\cdots}_{-\cdots}$	0.38
(f/r)[e]				$0.48^{+\cdots}_{-\cdots}$	0.30
		(1460^{+838}_{-864})	(605^{+309}_{-332})	$(12.82^{+3.46}_{-2.59})$	
				$(0.00^{+0.44}_{-0.00})$	0.38
				$(0.47^{+0.43}_{-0.21})$	0.30
S xvi L$_\alpha$	4.727	788^{+2914}_{-788}	795^{+614}_{-307}	$5.32^{+6.12}_{-4.79}$	
		(794^{+575}_{-539})	(773^{+223}_{-215})	$(5.24^{+2.66}_{-1.81})$	
S xv K$_\alpha$	5.039	265^{+646}_{-265}	-323^{+267}_{-115}	$12.10^{+4.81}_{-4.11}$	
(i/r)				$1.27^{+2.11}_{-0.69}$	0.23
(f/r)				$0.49^{+1.37}_{-0.49}$	0.44
		(186^{+592}_{-186})	(-356^{+13}_{-137})	$(11.83^{+2.89}_{-2.41})$	
				$(1.63^{+1.46}_{-0.61})$	0.23
				$(0.74^{+0.76}_{-0.34})$	0.44
Si xiv L$_\alpha$	6.180	1694^{+659}_{-1186}	-426^{+390}_{-327}	$3.99^{+2.01}_{-1.48}$	
		(1571^{+963}_{-684})	(-461^{+215}_{-222})	$(4.30^{+1.12}_{-1.10})$	
Si xiii K$_\alpha$	6.648	970^{+909}_{-875}	-346^{+268}_{-213}	$4.71^{+2.07}_{-1.76}$	
(i/r)				$0.00^{+0.22}_{-0.00}$	0.20
(f/r)				$1.03^{+1.01}_{-0.52}$	0.52
		(869^{+402}_{-372})	(-307^{+105}_{-115})	$(5.01^{+1.12}_{-0.96})$	
				$(0.00^{+0.11}_{-0.00})$	0.20
				$(1.07^{+0.52}_{-0.31})$	0.52

Notes. Results from the fits to the line profiles in the first-order MEG (Si xiii, Si xiv, S xv) and HEG (S xvi, Fe xxv) spectra with the associated 1σ errors (1σ error is equivalent to a change in the best-fit statistic value by 1). For the He-like triplets, the flux ratios of the intercombination to the resonance line (i/r) and of the forbidden to the resonance line (f/r) are given as well. The errors on the spectral parameters are those following the Gehrels (1986) recommendation for the cases with a small number of counts in individual data bins (see Section 2). When we enforced the Gaussian errors on the data (error = $\sqrt{N}$, N is the number of counts in a data bin), the results from the fits to the line profiles remained within 10%–15% of the values given in this table and the errors from the fits were 40%–60% of the values listed here. For comparison, the results from the fits based on the Cash statistic (Cash 1979) are given in parentheses.
[a] The laboratory wavelength of the main component
[b] The line width (FWHM)
[c] The shift of the spectral line centroid
[d] The observed total multiplet flux in units of 10^{-6} photons cm^{-2} s^{-1}
[e] Because of the poor photon statistics, these line ratios are not constrained.

previously discussed lines by introducing a common continuum for them, represented by bremsstrahlung emission with a plasma temperature $kT = 3$ keV. (Fits with a variable plasma temperature were equally successful.) The line profiles were modeled as done earlier—by a sum of two or three Gaussians for the doublet and triplet lines, respectively. This global-continuum fit provided line parameters that were identical to the ones given in Table 1. These consistency checks provide additional confidence in the derived spectral line parameters despite their relatively large uncertainties.

5. GLOBAL SPECTRAL FITS

The infrared variability of WR 48a suggests that it is a long-period dust maker; thus, it is likely a long-period WR+O binary system (Williams 1995; Williams et al. 2012). The *XMM-Newton* observation of its X-ray emission provided additional support for its suspected binary nature by discovering that WR 48a is a luminous X-ray source with high plasma temperature (Zhekov et al. 2011). All of these characteristics indicate that colliding stellar winds (CSWs) may play an important role in the physics of this object. We recall that as a result of CSWs, a two-shock structure forms between the two massive stars in the binary system. This structure is a source of X-ray emission (Prilutskii & Usov 1976; Cherepashchuk 1976), and it is believed to give rise to the variable infrared emission (dust emission; e.g., Williams et al. 1990). We will thus explore the CSW picture in the analysis of the *Chandra* spectra of WR 48a. The best way of doing this is to confront the results from hydrodynamic modeling of CSWs in WR 48a with the observations. However, basic physical parameters needed to construct a detailed model such as the stellar wind parameters and the binary separation are not available. We will therefore adopt a simplified approach on the basis of discrete-temperature plasma models. We emphasize that discrete-temperature models are a simplified representation of the temperature-stratified CSW region (for a discussion of CSW models versus discrete-temperature models, see Section 5.2 in Zhekov 2007). In this study and in our previous study of the X-ray emission from WR 48a (Zhekov et al. 2011), we adopted the discrete-temperature model *vpshock* in XSPEC. It is a physical model of the X-ray emission behind a strong plane-parallel shock that takes into account the effects of nonequilibrium ionization (for details of the model, see Borkowski et al. 2001).

As demonstrated in Section 3, apparent changes have occurred in the X-ray emission of WR 48a between 2008 January and 2012 October. In particular, the X-ray emission became weaker and more absorbed (Figure 1). Such changes are possible in the standard CSW picture even for steady-state stellar winds (i.e., mass-loss rates and wind velocities are constant in time). For example, if the orbital inclination is considerably higher than $0°$, then higher X-ray absorption should be detected for orbital phases when the star with the more massive wind in the binary is in front (e.g., at azimuthal angles around $\omega \approx 0°$; see Figure 4), In a WR+O binary, this occurs when the WR star is located between the observer and the CSW region. This change (increase) in absorption will occur when the WR star is in front regardless of whether the orbit is circular or elliptical. In contrast, the intrinsic X-ray luminosity of CSWs will change during the orbit only in the case where the orbit is elliptical. We recall that there exists a scaling law for the CSW X-ray luminosity with the mass-loss rate ($\dot{M}$), wind velocity (v), and binary separation (D): $L_X \propto \dot{M}^2 v^{-3} D^{-1}$ (Luo et al. 1990; Myasnikov & Zhekov 1993). We thus see that even for constant mass-loss rate and wind velocity, the intrinsic CSW luminosity will vary because of the change of the binary separation if the orbit is elliptical. L_X will reach its maximum near periastron (at the minimum value of D) and will have its minimum at apastron (the maximum value of D). We will next explore the CSW picture in the analysis of the *Chandra* spectra of WR 48a by assuming that (most of) its X-ray emission originates in CSWs.

We note that all of the global spectral models considered in this study have the following basic characteristics. Because no appreciable excess in the X-ray absorption above that expected from the interstellar medium was found in the analysis of

Figure 4. Schematic diagram of colliding stellar winds in a massive WR + O binary system. The wind interaction cone is denoted by CSW (the axis Z is its axis of symmetry; the axis X is perpendicular to the orbital plane; the axis Y completes the right-handed coordinate system). The line-of-sight toward the observer is denoted by l.o.s. and the two related angles; i (orbital inclination) and ω (azimuthal angle) are marked as well. The arrows labeled "velocity" indicate the general direction of the bulk gas velocity in the interaction region.

the *XMM-Newton* spectra of WR 48a, the column density of the interstellar X-ray absorption was kept fixed to $N_{\rm H,ISM} = 2.30 \times 10^{22}$ cm^{-2} (see Table 1 in Zhekov et al. 2011). The additional X-ray absorption that is observed in the *Chandra* spectra (see Section 3 and Figure 1) is attributed to the wind absorption in the more massive WR wind in the presumed WR + O binary. The vphabs model in XSPEC was used for this additional absorption component, and we enforced its abundances to be the same as that of the emission components. The chemical abundances of the emission components are with respect to the typical WC abundances (van der Hucht et al. 1986), and they were kept fixed to their values derived in Zhekov et al. (2011; see the 2T-shock model in Table 1 therein).[8] The following were the values (expressed as scaling factors to be applied to the typical WC abundances): He = 1, C = 1, N = 1, Ne = 0.11, Mg = 0.13, Si = 0.64, S = 1.78, Ar = 2.78, Ca = 1.97, and Fe = 1.31. In our analysis, the total (summed) first-order MEG and HEG spectra and the zeroth-order HETG spectra were fitted simultaneously. To improve the photon statistics, the spectra were re-binned to have a minimum of 20 counts per bin. On the basis of the results from the line profile analysis (Section 4), a typical line broadening of FWHM = 1000 km s^{-1} and a typical line shift of -365 km s^{-1} were assumed.

Let us now attribute the entire X-ray emission from WR 48a to the CSWs in a presumed WR + O binary. We recall that if the binary orbit is circular, no changes of the intrinsic X-ray parameters are expected with the orbital phase while the X-ray luminosity may vary if the orbit is elliptical. We denote these two cases as CSW$_{\rm circ}$ and CSW$_{\rm ell}$, respectively.

CSW$_{\rm circ}$. In this case, we made use of the two-shock model that successfully fitted the *XMM-Newton* spectra of WR 48a (see the 2T-shock model in Table 1 in Zhekov et al. 2011; the model uses the vpshock model in XSPEC in conjunction with the XSPEC command *xset neivers* 2.0 to select version

---

[8] Abundances in XSPEC are set by the *abund* command, which reads a default file that nominally contains the fractional abundance by number of each element relative to hydrogen (e.g., for solar abundances, H = 1.0 and He = 0.097). To simulate non-solar abundances for He-rich but H-depleted WC stars, the default abundance file is modified such that He is assigned a very high abundance relative to H (H = 1.0 and He = 50 in our simulations), and the remaining elements are then scaled to their appropriate number fractions relative to He on the basis of the values given in van der Hucht et al. (1986).

Table 2
Global Spectral Model Results

Parameter	CSW$_{circ}$	CSW$_{ell}$	1T Shock
χ^2/dof	1107/349	249/348	249/347
$N_{H,ISM}$ (10^{22} cm^{-2})	2.30	2.30	2.30
$N_{He,wind,1}$ (10^{21} cm^{-2})	$0.12^{+0.01}_{-0.01}$	$0.35^{+0.06}_{-0.14}$	$0.13^{+0.02}_{-0.01}$
$N_{He,wind,2}$ (10^{21} cm^{-2})	$2.65^{+0.11}_{-0.07}$	$0.12^{+0.16}_{-0.07}$	
kT_1 (keV)	1.05	1.05	$2.41^{+0.09}_{-0.14}$
kT_2 (keV)	2.82	2.82	
EM$_1$ (10^{54} cm^{-3})	2.42	$0.88^{+0.02}_{-0.02}$	$2.40^{+0.17}_{-0.04}$
EM$_2$ (10^{54} cm^{-3})	5.34	1.94	
τ_1 (10^{11} cm^{-3} s)	2.42	2.42	$15.9^{+6.70}_{-4.10}$
τ_2 (10^{11} cm^{-3} s)	8.09	8.09	
F_X (10^{-11} erg cm^{-2} s^{-1})	0.30 (17.7)	0.28 (6.44)	0.27 (2.09)
$F_{X,hot}$ (10^{-11} erg cm^{-2} s^{-1})	0.20 (6.98)	0.26 (2.53)	

Notes. Results from simultaneous fits to the *Chandra* HETG spectra (including both zeroth-order and first-order spectra) of WR 48a (the plasma model used in the fits is the *vpshock* model in XSPEC; see Section 5 for details). The abundances were with respect to the typical WC abundances (van der Hucht et al. 1986) and kept fixed to their values derived in Zhekov et al. (2011). Tabulated quantities are the neutral hydrogen absorption column density ($N_{H,ISM}$), the neutral helium absorption column density (wind absorption; $N_{He,wind}$), plasma temperature (kT), emission measure (EM $= \int n_e n_{He} dV$) for a reference distance of $d = 1$ kpc (EM $\propto d^2$), shock ionization age ($\tau = n_e t$), and the absorbed X-ray flux (F_X) in the 0.5–10 keV range followed in parentheses by the unabsorbed value ($F_{X,hot}$ denotes the higher-temperature component). Errors are the 1σ values from the fits.

2.0 of the nonequilibrium ionization collisional plasma model). All of the model parameters were kept fixed to their values as derived in that analysis. Because excess X-ray absorption is seen in the *Chandra* data (see Section 3 and Figure 1), the two-shock components suffer additional wind absorption as previously described. We first assumed that both emission components have equal wind absorptions. This resulted in a very poor-quality spectral fit (reduced $\chi^2 \approx 9$). If different X-ray absorptions for each component were allowed, the quality of the fit improved but was still statistically unacceptable (reduced $\chi^2 = 3.2$; see Table 2 for details). We can thus conclude that the physical picture of CSW in a WR + O binary that has a circular orbit is not supported by the X-ray observations of WR 48a. Such a picture cannot explain the observed changes in the X-ray emission from this object.

CSW$_{ell}$. In this case, we made use of the same model as previously described (CSW$_{circ}$), but we also allowed the shock emission measure to vary. This means that we assumed that the shape of the intrinsic X-ray emission does not change with the orbital phase, and only the amount of the X-ray emitting plasma does. In other words, although the distance between the stars in the binary varies, it does not become very small; therefore, the stellar winds still have enough space to reach their terminal velocities before they collide. We believe that this is a reasonable assumption for a wide binary system having a long period orbit as is likely the case with WR 48a (its orbital period is at least 32 yr; e.g., Williams et al. 2012). In the fitting procedure, we kept all of the shock plasma parameters fixed to their values in the original two-shock model (see the 2T-shock model in Table 1 in Zhekov et al. 2011). We allowed the total emission measure to vary, but we kept the ratio of the emission measures of the shock components fixed to its value as derived in the analysis of the *XMM-Newton* spectra. By fixing this ratio, the shape of the X-ray spectrum is not allowed to vary. Both models with a common (equal) or with a different X-ray absorption
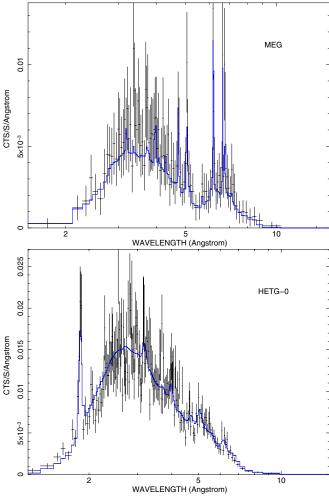
for each shock component gave very good fits to the observed *Chandra* HETG spectra. Figure 5 and Table 2 present the results for the case with a separate X-ray absorption for each emission component (i.e., for each shock). The model fit with equal wind absorptions had χ^2/dof = 251/349, and it gave identical plasma parameters with the ones presented in Table 2. The common wind absorption was practically a mean of the values given in that table, namely $N_{He,wind} = 0.16^{+0.01}_{-0.01} \times 10^{21}$ cm^{-2}. The basic result from the CSW$_{ell}$ case is that in 2012 October, the intrinsic X-ray emission (the amount/emission measure of hot plasma as well) of WR 48a was by a factor $\sim$3 lower than its value in 2008 January, and the level of the X-ray attenuation increased at the same time, as anticipated in Section 3.

In the framework of the standard CSW picture in a binary with an elliptical orbit, the lower X-ray luminosity should be observed when the binary separation is larger. This means that the orbital orientation of WR 48a is such that in 2012 October, the binary separation was larger than it was in 2008 January. To have an increased value of the X-ray attenuation, the star with the more massive wind should be nearly in front in 2012 October (i.e., azimuthal angles around $\omega \approx 0°$; see Figure 4), so then its counterpart was likely in front in 2008 January (i.e., azimuthal angles around $\omega \approx 180°$; see Figure 4). This seems to be the case given that the X-ray absorption (neutral hydrogen column density) showed no appreciable excess above the interstellar value in 2008 January (Zhekov et al. 2011). However, if the WR star is in front, the plasma in the interaction region will be outflowing (see Figure 4)—that is, it is moving away from the observer. Because the WR wind is expected to be dominant in the system, the apex of the CSW cone will point toward the WR star (and toward the observer as well). Instead, we found blueshifted spectral lines in the X-ray spectrum of WR 48a in 2012 October (see Section 4), which indicates that the X-ray emitting plasma was moving toward the observer. This suggests that the star with the weaker wind was in front at the time of the *Chandra* observation in 2012 October (i.e., azimuthal angles around $\omega \approx 180°$; see Figure 4). We will return to this apparent discrepancy in Section 6.

6. DISCUSSION

The following are the most important results from the analysis of the *Chandra* HETG spectra of WR 48a: (1) blueshifted and broadened (spectrally resolved) emission lines are detected; (2) in 2012 October, the emission measure of the hot gas is about a factor of $\sim$3 lower than it was in 2008 January; (3) the X-ray absorption has increased considerably over the same period of time.

As discussed in Section 5, the CSW picture was adopted in our analysis of the entire X-ray emission from WR 48a. It was done in a simplified manner by making use of a two-shock model. We recall that the CSW region is temperature-stratified, and the two-temperature plasma (two-shock model) is just a simplified representation of the temperature stratification of its hot plasma weighted by its emission measure. Thus, we believe that the results derived from the two-shock modeling (the last two that were previously mentioned) are definitely valid in the CSW picture. To double-check these two results, we also fitted the HETG spectra with a one-shock model. The results from this model fitting also confirmed the decrease of emission measure by the same factor ($\sim$3) and the increased (wind) absorption (see 1T-shock model in Table 2). The single-temperature shock model in this case is successful because the X-ray spectrum of WR 48a is heavily absorbed. However,
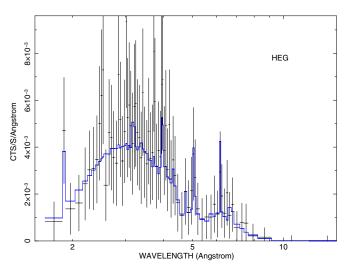
Figure 5. HETG background-subtracted spectra of WR 48a and the two-component model fit (see model CSW$_{ell}$ in Table 2). The spectra were re-binned to have a minimum of 20 counts per bin.

(A color version of this figure is available in the online journal.)

we have given preference to the two-shock model in our analysis (Section 5) for consistency with the previous study of the X-ray emission of WR 48a, in which a two-shock model was required to match the observed spectra successfully (Zhekov et al. 2011).

As previously mentioned, each of the three most important results from this study can be explained in the framework of the CSW picture. In particular, the blueshifted emission lines indicate that the star with the less powerful wind was globally in front of the CSW region at the time of the *Chandra* observation. In contrast, the decrease of the emission measure over a period of almost 5 yr is a sign of an elliptical orbit in the presumed WR + O binary system. Last, the increased X-ray absorption in 2012 October compared to that in 2008 January indicates that we observed the X-ray emission from the CSW region through a massive stellar wind in the former and likely through the hot gas of the CSW region (or at an orbital phase far from conjunction, and thus, no wind absorption) in the latter. However, can we get simultaneously these three observational facts to be consistent with the CSW picture? We believe it is possible in the following—although speculative—way.

Suppose the binary system in WR 48a consists of two massive stars: a WR star (of the WC subtype) being the primary in the system and a secondary star that is not an O star but rather a WR or a luminous blue variable star. (The latter luminous blue variable case might be an object similar to the Small

Magellanic Cloud star HD 5980; see Koenigsberger et al. 2010 and references therein.) Suppose the stellar wind of the WC primary is more powerful than that of the secondary. In the case of an elliptical orbit, the decrease of the emission measure of the CSW region between 2008 January and 2012 October is then explained by the increase of the binary separation over that period of time. If the secondary star was in front (e.g., azimuthal angles around $\omega \approx 180°$; see Figure 4) at the time of the *Chandra* observation (2012 October), then this would explain the detection of blueshifted lines in the spectrum of WR 48a. In contrast, if the secondary is a WR or luminous blue variable star, the high X-ray wind absorption is also expected at this orbital phase provided the orbital inclination is high enough. If the latter is close to $90°$ and the orbital phase at which the secondary is in front has not yet passed, the X-ray absorption will keep increasing. Alternatively, if that orbital phase has already passed, the X-ray absorption is already beyond its maximum and it will decrease in the future. This would be a secondary maximum for the X-ray absorption given that its primary maximum will occur when the primary star (WC) is in front (e.g., azimuthal angles around $\omega \approx 0°$; see Figure 4). To explain the low (negligible) wind absorption in the 2008 January *XMM-Newton* observation, we should assume that at that time, we observed the CSW region through its hot gas. This means that the line of sight intercepted the CSW cone itself (bounded by

the two-shock surfaces), which eliminates the wind absorption. If this were the case, we may expect that after the phases with increased X-ray absorption have passed, we will witness another phase with low wind absorption, which will allow us to directly estimate the opening angle of the CSW cone. The chemical composition of the absorbing wind cannot be constrained from the X-ray data alone. We recall that, in our analysis, the wind absorption component and the emission component share the same abundances. However, successful fits to the HETG spectra were possible even if we assumed that the wind absorption component had a chemical composition typical for interstellar matter. Therefore, our suggestion that the secondary star in the binary might be a WR or a luminous blue variable star does not conflict with the data. Nevertheless, deep high-resolution optical observations are essential to validate this suggestion.

We note that the observed changes in the X-ray emission of WR 48a between 2008 January and 2012 October might be the result of some temporary state of the binary system (e.g., they could be a consequence of time-variable stellar wind parameters). Asymmetric stellar winds, having an appreciable contrast of the wind parameters between the stellar pole and equator, could also contribute to those changes. Also, WR 48a could be a system of higher hierarchy than just a wide binary system with a period of $\geqslant$32 yr as proposed by Williams et al. (2012). To interpret the data at hand, such explanations seem more speculative to us than the one previously described. As in the *XMM-Newton* data (Zhekov et al. 2011), we found no short-term variability in the *Chandra* data of WR 48a. On a timescale less than 100 ks and time bins between 100 and 2000 s, the X-ray light curve is statistically consistent with a constant flux. In contrast, even if the physical picture behind the X-ray emission from WR 48a were more complicated than just CSWs, the latter is likely one of its important ingredients. The strong forbidden line in the He-like triplet of Si XIII (Table 1) is a solid indicator that this line complex forms in a rarefied hot plasma far from strong ultraviolet sources, which clearly points to a CSW region in a wide massive binary system. It is worth noting that the other He-like triplet detected in the WR 48a spectra, namely S XV, shows enhanced emission from the intercombination line, which may indicate a different origin of the very hot plasma where the S XV line complex forms. However, as already mentioned (Section 4), the data in that part of the spectrum are of lower quality, and a deeper observation would be needed to validate this result.

7. CONCLUSIONS

In this work, we presented an analysis of the first grating X-ray spectra of the dusty WR star WR 48a obtained with the *Chandra* HETG. The basic results and conclusions are as follows.

1. From analysis of the line profiles of strong emission lines, a typical line width (full width at half maximum) of 1000–1500 km s^{-1} was deduced and blueshifted line centroids of $\sim$−360 km s^{-1}. A strong (not suppressed) forbidden line in the He-like triplet of Si XIII was detected, which indicates that this line forms in a rarefied hot plasma far from strong sources of ultraviolet emission.
2. Global spectral modeling showed that the X-ray spectrum of WR 48a suffered higher absorption (likely of wind origin) in 2012 October (the *Chandra* observation) compared with 2008 January (the *XMM-Newton* observation). The

emission measure of the hot plasma in WR 48a decreased by a factor $\sim$3 over the same period of time.
3. No X-ray variability on a timescale of less than 100 ks was detected. This result is similar to what was found from the analysis of the previous X-ray observation of WR 48a with *XMM-Newton* (Zhekov et al. 2011).
4. The most likely physical picture that emerges from the analysis of the available X-ray data (*Chandra* and *XMM-Newton*) is the following. The high X-ray luminosity of the carbon-rich WR star WR 48a is the result of CSWs in a wide binary system with elliptical orbit. The observed changes of the characteristics (emission measure, absorption) of the X-ray emission of WR 48a and the blueshift of the line centroids of the strong lines can find their place in the CSW picture, provided the secondary star in the binary system (the companion star of the primary WC object) is not an O star but instead a WR star or a luminous blue variable star.
5. More X-ray observations with high spectral resolution are needed to describe in detail the X-ray characteristics of WR 48a. Because of the high X-ray absorption of this object (most of the X-ray emission from WR 48a emerges at energies above 2 keV), *Chandra* HETG data are essential for us to obtain a deeper understanding of the physical picture of CSWs in the fascinating dusty WR star WR 48a.

REFERENCES

Arnaud, K. A. 1996, in ASP Conf. Ser. 101, Astronomical Data Analysis Software and Systems, ed. G. Jacoby & J. Barnes (San Francisco, CA: ASP), 17
Baume, G., Carraro, G., & Momany, Y. 2009, MNRAS, 398, 221
Borkowski, K. J., Lyerly, W. J., & Reynolds, S. P. 2001, ApJ, 548, 820
Cash, W. 1979, ApJ, 228, 939
Cherepashchuk, A. M. 1976, SvAL, 2, 138
Danks, A. C., Dennefeld, M., Wamsteker, W., & Shaver, P. A. 1983, A&A, 118, 301
Danks, A. C., Wamsteker, W., Shaver, P. A., & Retallack, D. S. 1984, A&A, 132, 301
Dougherty, S. M., & Williams, P. M. 2000, MNRAS, 319, 1005
Gehrels, N. 1986, ApJ, 303, 336
Hindson, L., Thompson, M. A., Urquhart, J. S., et al. 2012, MNRAS, 421, 3418
Koenigsberger, G., Georgiev, L., Hillier, D. J., et al. 2010, AJ, 139, 2600
Luo, D., McCray, R., & MacLow, M.-M. 1990, ApJ, 362, 267
Myasnikov, A. V., & Zhekov, S. A. 1993, MNRAS, 260, 221
Oskinova, L. M., Ignace, R., Hamann, W.-R., Pollock, A. M. T., & Brown, J. C. 2003, A&A, 402, 755
Prilutskii, O. F., & Usov, V. V. 1976, SvA, 20, 2
Skinner, S. L., Güdel, M., Schmutz, W., & Zhekov, S. A. 2006, Ap&SS, 304, 97
van der Hucht, K. A. 2001, NewAR, 45, 135
van der Hucht, K. A., Cassinelli, J. P., & Williams, P. M. 1986, A&A, 168, 111
Williams, P. M. 1995, in IAU Symp. 163, Wolf-Rayet Stars: Binaries, Colliding Winds, Evolution, ed. K. A. van der Hucht & P. M. Williams (Dordrecht: Kluwer), 335
Williams, P. M., van der Hucht, K. A., Pollock, A. M. T., et al. 1990, MNRAS, 243, 662
Williams, P. M., van der Hucht, K. A., van Wyk, F., et al. 2012, MNRAS, 420, 2026
Zhekov, S. A. 2007, MNRAS, 382, 886
Zhekov, S. A., Gagné, M., & Skinner, S. L. 2011, ApJL, 727, L17